JOURNAL OF AIRCRAFT
Vol. 35, No. 3, May–June 1998

Active Control of Store-Induced Flutter in Incompressible Flow

Prasad V. N. Gade* and Daniel J. Inman†
Virginia Polytechnic Institute and State University, Blacksburg, Virginia 24061

An active method for enhancing the performance and improving the robustness of a decoupler pylon-mounted store flutter suppression system is presented. The proposed active decoupler pylon involves the use of a piezoceramic wafer strut as an actuator that acts as a soft spring between the wing and the store. A two degree-of-freedom typical section of an airfoil is used to represent the structural model of the wing. The circulatory component of the incompressible aerodynamic loads is modeled using an approximation to the Theodorsen function. The GBU-8/B store configuration of an F-16 aircraft is used for the analysis. A classical robust control algorithm called the loop transfer recovery method is applied to design a controller for the linear wing/store model. Some simulations are presented using singular-value Bode plots for robust stability and nominal performance analysis.

Nomenclature

ab = distance between elastic center and midchord
b = semichord length
h = plunge displacement
i = $\sqrt{-1}$
$l_1 b$ = distance between top of strut to elastic center
$l_2 b$ = distance between pivot point to elastic center
m_a = mass of the piezoceramic wafer actuator per unit length
m_f = fictitious noise-intensity coefficient
m_s = mass of the store
m_w = mass of the wing
$r_\alpha b$ = radius of gyration of airfoil about elastic axis
$r_\theta b$ = radius of gyration of pylon/store about pivot point
$S(s)$ = sensitivity function
s = Laplace variable
$\bar{s}$ = reduced frequency, bs/U
$T(s)$ = complementary sensitivity function
$T(\bar{s})$ = Theodorsen function
U = freestream velocity
U_f = flutter speed
u = actuator output, control moment
w = external disturbance
$x_\alpha b$ = distance between elastic center and c.g. of wing
$x_\theta b$ = distance between c.g. of store to pivot point
x_1, x_2 = aerodynamic lag states
α = pitch angle of airfoil
$\Delta_{\text{im}}(s)$ = input multiplicative uncertainty transfer function
θ = store pitch angle relative to wing
ρ = air density
$\underline{\sigma}$ = minimum singular value
$\overline{\sigma}$ = maximum singular value
ω_h = uncoupled wing bending frequency
ω_α = uncoupled wing torsional frequency
ω_θ = uncoupled store pitch frequency

Received Aug. 11, 1996; revision received July 30, 1997; accepted for publication Nov. 12, 1997.

*Graduate Research Assistant, Department of Engineering Science and Mechanics. Student Member AIAA.

†Herrick Endowed Professor, Department of Engineering Science and Mechanics. Associate Fellow AIAA.

Introduction

A TOPIC of current interest in the aeronautical community is the flutter suppression of high-performance combat aircraft carrying underwing stores. Fighter aircraft are required to carry several combinations of external stores and perform maneuvers in a variety of flight conditions. The increase in weight caused by the addition of the store decreases the frequency of the first torsional mode of the wing, thereby bringing it closer to the fundamental bending frequency. This coupling between bending and torsional modes results in a substantial decrease in flutter speed. Although passive methods such as structural and mass balance techniques have claimed to alleviate flutter, the associated added weights generally result in decreased aircraft performance. Moreover, the requirement on the aircraft to carry several combinations of stores makes its implementation practically impossible. The increasing restrictions on weight together with high-performance requirements places active control technology at an advantage, particularly with the development of new tools in evaluating robustness issues.

This paper uses a linear quadratic Gaussian/loop transfer recovery (LQG/LTR) control technique to investigate the robust stability and nominal performance issues associated with the compensated wing/store flutter suppression model of an airfoil in incompressible flow. Singular value plots of robust stability and performance measures as a function of frequency are used for the analysis.

Background and Motivation

Flutter can be alleviated by conventional passive schemes or by the more advanced active approaches. Passive methods typically include adding mass ballast, relocating store location spanwise and/or chordwise, or tuning the pylon stiffness characteristics.[1] These methods are generally tailored to a specific configuration and fail to accommodate different store mass and location combinations.

Active methods, on the other hand, are relatively more flexible and require mere change of control law to accommodate different store combinations. One of the earliest known works on the feasibility of using active control for wing/store flutter suppression was reported by Triplett.[2] His analytical study of an F-4 Phantom aircraft wing/store configuration involved deflecting ailerons in a manner to produce aerodynamic forces that opposed the flutter causing aerodynamic forces. A number of other investigators made important contributions to the field of active wing/store flutter suppression.[3,4] Harvey et al.[5] in-

vestigated the feasibility of using adaptive control for wing/store flutter suppression with the preceding approach. Some researchers[6,7] proposed a slightly modified version that involved feeding back signals from the accelerometers at the fore and aft end of the store to electrohydraulic actuators to drive vanes attached to the forward part of the store. The deflected vanes generated counteracting aerodynamic forces that stabilized the store pitch motion. Hönlinger and Destuynder[8] used a linear quadratic regulator (LQR) control law to test the preceding procedure on a Phantom F-4F wing/store configuration. The effectiveness of these methods, however, depended largely on the accurate knowledge of counteracting unsteady aerodynamic forces produced by the control surfaces. This poses a particular problem, particularly in the transonic range where the theoretical predictions of the unsteady aerodynamic coefficients of the control surfaces are least reliable.[9]

Triplett's feasibility study[2] gained interest in the aeronautical community and was soon followed by a U.S. Air Force contract to evaluate the ability of a single wing/store flutter-control scheme that would be robust to several different store configurations.[10] Instead of using control surface's unsteady aerodynamics as in the earlier active methods, Triplett and his colleagues proposed using a hydraulic actuator to decouple the store vibratory motion from that of the wing. Although the dynamic behavior of this scheme worked quite well in restoring bare wing flutter speed, the actuator's inability to meet high-flow-rate requirements for the control of higher frequency perturbations restricted its practical implementation.

Reed et al.[9] proposed a modified version of the previously mentioned approach. Instead of using a hydraulic actuator as a load-carrying tie, a passive soft-spring/damper combination was used together with a low-power active control system to maintain store alignment. Their idea is based on the argument that instead of modifying the aerodynamic forces, the frequencies associated with flutter critical bending and torsion modes can be separated by making the wing insensitive to store pitch inertia and eventually alleviate the adverse coupling to a higher flutter speed.

The design of the decoupler pylon-mounted store consists of a pitch–pivot mechanism near the fore end that allows the store to pitch relative to the wing surface. Near the aft end, a soft spring is used to decouple the influence of store pitch inertia on wing torsion modes. A low-frequency feedback control is used to prevent large static deflections and maintain alignment. The result is a substantial increase in flutter speed, well beyond that of the bare wing. The decoupler pylon concept was later successfully implemented on an F-16 aircraft to demonstrate the increase in flutter speed.[11]

Instead of passive soft-spring/damper elements as used by Reed et al.,[9] to demonstrate their concept, the current approach proposes an active decoupler pylon for the control of wing/store flutter suppression. The proposed active isolation scheme (Fig. 1), serves two purposes. First it decouples the wing dynamics from the store pitch inertia effects—a primary source for bending-torsion flutter in wing with external stores. Second, with the aid of a robust controller, it acts as an actuator that stabilizes and maintains the performance characteristics of the closed-loop system in the face of uncertainties at flutter speed. The active pylon consists of a strut with a series of thin circular plates laminated on opposite faces with piezoceramic material. The poled directions of the piezoceramics are aligned so that a voltage (control input) applied across the element contracts on one side and expands on the other. The plate bending is then translated into an axial motion along the strut. The piezostrut is designed such that its equivalent stiffness satisfies Reed's criterion of a soft spring system for isolation purposes, i.e., the store pitch to wing bending frequency ratio should always be less than 1 for effective store flutter alleviation. The novelty in this approach is the use of the strut as both a passive isolator as well as an active actuator to maintain stability and performance. The current active concept has two

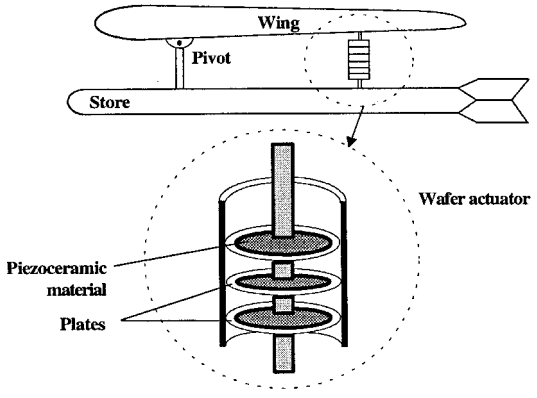

Fig. 1 Wing/store piezostrut arrangement.

major advantages over other passive schemes.[9,11] Not only does the active decoupler make the system more robust to various uncertainties, but it also has significant weight benefits because it gets away with all of the hardware that is required with pneumatic springs and hydraulic dashpots. Moreover, compared to that of a hydraulic actuator, wafer actuator's faster time response to input command signals makes it suitable for the store flutter suppression problem.

It is proposed that this device will represent a significant improvement in the much-needed stroke length requirement over the traditional stack actuator,[12] which has been shown to fail in providing the much-needed stroke length for restoring the bare wing flutter speed. Moreover, these actuators typically fail in tension because of the brittle nature of the piezoceramic materials. On the other hand, the current bender-element-type actuator, initially fabricated and designed[13] for use in a large flexible structure, behaves the same both in tension as well in compression. Several issues pertaining to the actuator are yet to be quantified such as actuator dynamics, its time response to input command signals relative to hydraulic actuators, stroke length capability over traditional stack actuators, and power requirements. At the time of writing of this paper, the dynamics of the actuator had not been identified and, hence, are not included.

In this paper, a controller for the wing/store flutter suppression model of an F-16 aircraft with a GBU-8/B store configuration is designed using a robust LQG/LTR technique. The wing is modeled using a two-dimensional approximation of a typical section of an airfoil and the store flutter problem is studied in incompressible flow regime. The objective is to design a closed-loop control system that is robust to various uncertainties, such as store aerodynamics and other flexible structural modes not taken into account in the model. Singular-value analysis is used to assess the system's nominal performance and robust stability characteristics in the face of such uncertainties.

Plant Description

The analytical model is restricted to a typical section of a thin airfoil with an underwing store in two-dimensional incompressible flow. A sketch of the typical section together with the decoupler pylon and the store is shown in Fig. 2.

The plunging or bending motion of the entire airfoil/store combination together with pitch angles of the lifting surface α and the store θ measured relative to the wing constitute the three degrees of freedom of the wing/store model. Linear and torsional springs at the elastic center are used to model the restraining forces generated by the vertical and angular displacements of the airfoil, whereas restraint to the pitching motion of the store is provided by the decoupler pylon mechanism. Standard sign conventions are used in which the plunging displacement is measured positive downward while a nose-up position of the structure implies a positive pitching angle. The total lift on the airfoil is defined positive-up while the pitching

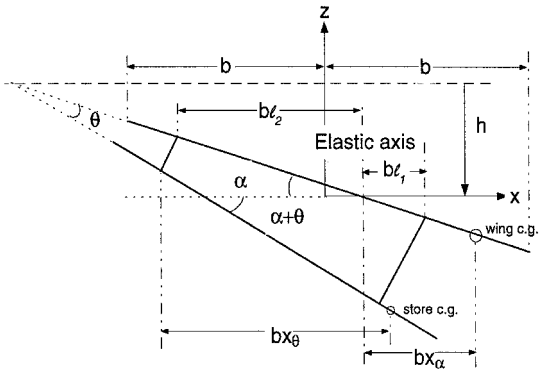

Fig. 2 Schematic diagram of a thin airfoil and decoupler pylon-mounted store.

moment of the entire airfoil about the one-quarter chord length point is positive in the nose-heavy sense. Assuming no structural damping, the equations of motion in the time domain are given by

$$\boldsymbol{M}_s\ddot{\boldsymbol{q}} + \boldsymbol{K}_s\boldsymbol{q} = \begin{Bmatrix} -L_{\text{aero}} \\ M_{\text{aero}} \\ 0 \end{Bmatrix} \tag{1}$$

where

$$\boldsymbol{q}(t) = \{h/b \;\; \alpha \;\; \theta\}^T$$

is a vector of generalized coordinates in which the plunge motion h of the airfoil is nondimensionalized by b to enable easy comparison with the pitching motions. The left-hand side of Eq. (1) consists of the mass and elastic terms of the airfoil, the actuator, and the attached store, and are given as

$$\boldsymbol{M}_s = \begin{bmatrix} \mu_w + \mu_s + \mu_a & \mu_w x_\alpha + \mu_a l_1 + \mu_s(x_\theta - l_2) & \mu_s x_\theta + \tfrac{1}{2}\mu_a l_1 \\ \mu_w x_\alpha + \mu_a l_1 + \mu_s(x_\theta - l_2) & \mu_w r_\alpha^2 + \mu_a l_1^2 + \mu_s(r_\theta^2 + l_2^2 - 2x_\theta l_2) & \mu_s(r_\theta^2 - x_\theta l_2) + \tfrac{1}{2}\mu_a l_1^2 \\ \mu_s x_\theta + \tfrac{1}{2}\mu_a l_1 & \mu_s(r_\theta^2 - x_\theta l_2) + \tfrac{1}{2}\mu_a l_1^2 & \mu_s r_\theta^2 + \tfrac{1}{3}\mu_a l_1^2 \end{bmatrix}$$

$$\boldsymbol{K}_s = \begin{bmatrix} \mu_w\omega_h^2 & 0 & 0 \\ 0 & \mu_w r_\alpha^2\omega_\alpha^2 & 0 \\ 0 & 0 & \mu_s r_\theta^2\omega_\theta^2 \end{bmatrix} \tag{2}$$

where $\mu_w = m_w/\pi\rho b^2$, $\mu_s = m_s/\pi\rho b^2$, and $\mu_a = m_a L_a/\pi\rho b^2$ are the normalized masses of the wing, store, and the actuator respectively. Here, structural damping is neglected and the gravitational effects are ignored. The terms on the right-hand side (RHS) of Eq. (1) correspond to the aerodynamics identified as the lift L_{aero} and the moment M_{aero} per semichord length for a unit width span. A method for calculating the aerodynamic loads caused by simple harmonic oscillations of a wing section in incompressible flow was first given by Theodorsen.[14] The theory was then extended to arbitrary motions by Edwards.[15] His generalized unsteady aerodynamic theory divides the loads into noncirculatory and circulatory parts, and are expressed in the Laplace domain as

$$\begin{Bmatrix} -L_{\text{aero}} \\ M_{\text{aero}} \\ 0 \end{Bmatrix} = (-s^2\boldsymbol{M}_{\text{nc}} - s\boldsymbol{C}_{\text{nc}} + s\boldsymbol{C}_c + \boldsymbol{K}_c)\boldsymbol{q}(s) \tag{3}$$

where $\boldsymbol{M}_{\text{nc}}$ and $\boldsymbol{C}_{\text{nc}}$ are apparent additional mass and damping matrices caused by noncirculatory oscillations of the aerodynamic loads given by

$$\boldsymbol{M}_{\text{nc}} = \begin{bmatrix} 1 & -a & 0 \\ -a & a^2 + \tfrac{1}{8} & 0 \\ 0 & 0 & 0 \end{bmatrix}, \qquad \boldsymbol{C}_{\text{nc}} = \frac{U}{b}\begin{bmatrix} 0 & 1 & 0 \\ 0 & \tfrac{1}{8} - a & 0 \\ 0 & 0 & 0 \end{bmatrix} \tag{4}$$

while $\boldsymbol{C}_c$ and $\boldsymbol{K}_c$ matrices correspond to the circulatory part that are further subdivided into

$$s\boldsymbol{C}_c + \boldsymbol{K}_c = T(\bar{s})\boldsymbol{R}[s\boldsymbol{S}_2 + \boldsymbol{S}_1] \tag{5}$$

where

$$\boldsymbol{R} = \begin{Bmatrix} -2 \\ 2(a + \tfrac{1}{2}) \\ 0 \end{Bmatrix}, \qquad \boldsymbol{S}_1 = [0 \;\; 1 \;\; 0], \qquad \boldsymbol{S}_2 = [1 \;\; \tfrac{1}{2} - a \;\; 0]$$

In Eq. (5), $T(\bar{s})$ represents the complex Theodorsen function where $\bar{s} = b\omega i/U$ is a Laplace operator associated with nondimensional time Ut/b. The effects of aerodynamics on the store are, however, neglected to make the analysis simpler. With the aid of multivariable robust control techniques, the influence of unmodeled dynamics on the stability and nominal performance of the wing/store flutter suppression system are evaluated in the following text. The complete equations of motion are recast into the form

$$\{s^2(\boldsymbol{M}_s + \boldsymbol{M}_{\text{nc}}) + s\boldsymbol{C}_{\text{nc}} + \boldsymbol{K}_s\}\boldsymbol{q}(s) = T(\bar{s})\boldsymbol{R}[s\boldsymbol{S}_2 + \boldsymbol{S}_1]\boldsymbol{q}(s) + \boldsymbol{H}u(s) + \boldsymbol{F}\boldsymbol{w}(s) \tag{6}$$

where the term $\boldsymbol{w}$ represents the freestream airflow disturbance acting through an identity matrix, while u represents the actuator input acting through the input matrix $\boldsymbol{H} = [0 \;\; 0 \;\; 1]^T$. To complete the model in the Laplace domain, Jones'[16] second-order rational approximation to the complex Theodorsen function is used and is given by

$$T(\bar{s}) = \frac{0.5(sb/U)^2 + 0.2808(sb/U) + 0.01365}{(sb/U)^2 + 0.3455(sb/U) + 0.01365} \tag{7}$$

A nonunique state–space representation of Jones' approximation for unsteady circulatory aerodynamic load can be obtained as

$$\left[\begin{array}{c|c} \boldsymbol{A}_2 & \boldsymbol{B}_2 \\ \hline \boldsymbol{C}_2 & \boldsymbol{D}_2 \end{array}\right] = \left[\begin{array}{cc|c} -0.3(U/b) & 0 & -1.2650(U/b) \\ 0 & -0.0455(U/b) & -0.4927(U/b) \\ \hline -0.0799 & -0.0151 & 0.5 \end{array}\right] \tag{8}$$

The state–space representation of the structural equations and noncirculatory components of the aerodynamic loads is given as

$$\left[\begin{array}{c|c} \boldsymbol{A}_1 & \boldsymbol{B}_1 \\ \hline \boldsymbol{C}_1 & \boldsymbol{D}_1 \end{array}\right] = \left[\begin{array}{cc|c} \boldsymbol{0} & \boldsymbol{I} & \boldsymbol{0} \\ -(\boldsymbol{M}_s + \boldsymbol{M}_{\text{nc}})^{-1}\boldsymbol{K}_s & -(\boldsymbol{M}_s + \boldsymbol{M}_{\text{nc}})^{-1}\boldsymbol{C}_{\text{nc}} & (\boldsymbol{M}_s + \boldsymbol{M}_{\text{nc}})^{-1}\boldsymbol{R} \\ \hline (U/b)^2\boldsymbol{S}_1 & (U/b)\boldsymbol{S}_2 & \boldsymbol{0} \end{array}\right] \tag{9}$$

From Eq. (8), it is evident that the circulatory aerodynamic loads introduce two additional states, called the aerodynamic lags (x_1 and x_2), which increase the total number of states to eight. The state–space representation of the augmented system is given by

$$\boldsymbol{x} = \boldsymbol{A}\boldsymbol{x} + \boldsymbol{B}u + \boldsymbol{\Gamma}\boldsymbol{w}$$
$$\boldsymbol{y} = \boldsymbol{C}\boldsymbol{x} + \boldsymbol{D}u \tag{10}$$

where

$$\boldsymbol{x} = \{h/b \;\; \alpha \;\; \theta \;\; \dot{h}/b \;\; \dot{\alpha} \;\; \dot{\theta} \;\; x_1 \;\; x_2\}^T$$

$$\left[\begin{array}{c|c} \boldsymbol{A} & \boldsymbol{B} \\ \hline \boldsymbol{\Gamma}^T & \boldsymbol{D} \end{array}\right] = \left[\begin{array}{cc|c} \boldsymbol{A}_1 + \boldsymbol{B}_1\boldsymbol{D}_2\boldsymbol{C}_1 & \boldsymbol{B}_1\boldsymbol{C}_2 & \boldsymbol{B}_0 \\ \boldsymbol{B}_2\boldsymbol{C}_1 & \boldsymbol{A}_2 & \boldsymbol{0} \\ \hline \boldsymbol{E} & \boldsymbol{0} & \boldsymbol{0} \end{array}\right]$$

where $\boldsymbol{B}_0 = [\boldsymbol{0} \;\; (\boldsymbol{M}_s + \boldsymbol{M}_{nc})^{-1}\boldsymbol{H}]^T$, and $\boldsymbol{E} = [0 \;\; (\boldsymbol{M}_s + \boldsymbol{M}_{nc})^{-1}\boldsymbol{F}]^T$. The three primary outputs of interest are the plunging motion h, the wing pitch α, and the store pitch angle θ.

The following parameters represent those of an F-16 aircraft wing/store model with the GBU-8/B weapon system[11] and are used for the current simulation ($\rho = 4.2538$ kg/m^3): m_s = 1027.6 kg (2265 lb), $m_w = 5.3m_s$, m_aL_a = 13.61 kg (30 lb), $r_\alpha b$ = 0.635 m (25 in.), $r_\theta b$ = 0.830 m (32.7 in.), b = 1.12 m (44 in.), $\omega_\theta/\omega_h = 0.55$, $x_\alpha b$ = 0.178 m (7.04 in.), $x_\theta b = 0$, $l_1 b$ = 0.223 m (8.8 in.), $l_2 b$ = 0.223 m (8.8 in.), $ab = -0.1702$ m (-6.68 in.), ω_h = 24.5 rad/s, and $\omega_\alpha/\omega_h = 1.27$. Figure 3 shows the bending–torsion frequency coalescence trend as a function of airspeed. It illustrates the effectiveness of the decoupler pylon-mounted wing/store system over a rigidly mounted store in increasing the flutter speed. The frequencies at ground speed are those from the undamped, inertially coupled wing/store system that is slightly reduced because of the apparent additional mass contributed by the noncirculatory component of the aerodynamic loads [Eq. (6)]. As the flight speed increases, the bending branch frequency for both rigid and decoupler case remains approximately equal to its ground frequency, with a slight increase near the flutter speed. The first wing–torsional mode frequency for the decoupler case, however, decreases relatively less than that corresponding to the rigid case because of the reduced store–pitch inertia effects (due to the presence of soft spring-like actuator), and comes close to the bending branch near the flutter speed. The result is an increase in flutter speed for the decoupler-mounted store system. These branches do not coalesce because of the presence of aerodynamic damping present in the system.

The open-loop flutter speed is therefore predicted exactly from the V-g plot by calculating the speed where dissipation energy changes sign. The variation of bending and torsional mode structural damping as a function of airspeed is shown in Fig. 4. It is observed that for both torsional and bending modes, the damping initially increases with airspeed along

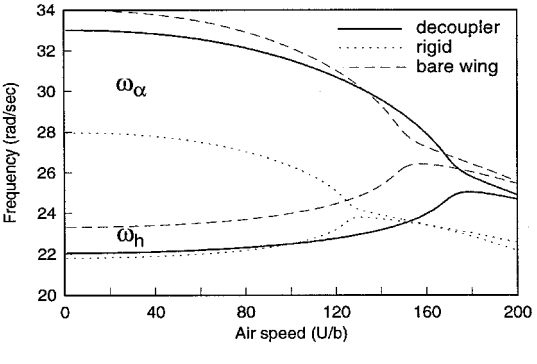

Fig. 3 Bending–torsion frequency coalescence vs airspeed.

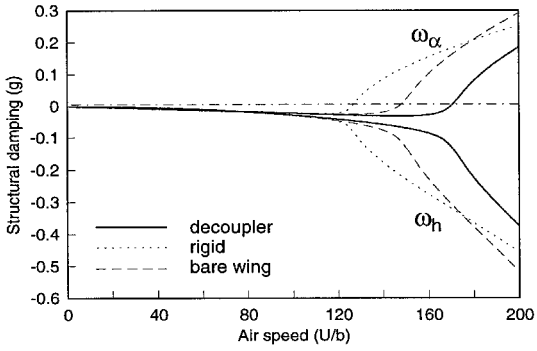

Fig. 4 Structural damping vs airspeed.

with the one corresponding to the bending branch, increasing much more rapidly than the torsional branch. At about 85–95% of the flutter speed, the torsional mode damping suddenly decreases and approaches zero at the flutter speed. The bending mode damping, however, continues to increase at a much faster rate. The open-loop flutter speed where the torsional mode damping changes sign is found to occur at U/b = 170 for the decoupler case and U/b = 127 for the rigid case. For comparison, the flutter speed for a clean wing (without any store) is found to be at U/b = 148. This represents a 14.86% increase in flutter speed with decoupler pylon over that of a bare wing and a 33.86% increase over a rigidly attached case.

Uncertainty Representation

The dynamics of any physical system can never be captured completely by mathematical models. There are always errors associated with the approximations made during the modeling process. These approximations are made either because of the lack of complete knowledge of the system or because of difficulty in modeling. For instance, the plant described in the previous section does not include actuator dynamics and aeroloads on the store are neglected. These imprecisions in high-frequency dynamics are termed as unstructured uncertainties that generally result in an underestimation of the system order. Some of the other examples of unstructured uncertainties for a wing/store flutter problem are the errors resulting from ignoring rigid body modes of the aircraft.

Uncertainties can also be parametric in nature where the parameters fluctuates slowly between known values. These low-frequency perturbations are called structured uncertainties. In the case of wing/store flutter problem, they are common in situations of combat when the c.g. location and the radius of gyration of the store vary with various rigid body maneuvers. Hence, during the design of an appropriate controller, the robustness of the closed-loop system in the face of these uncertainties and maintenance of its nominal performance are therefore the primary objectives of any control strategy.

In robust control literature, the mathematical representation of uncertainties caused by such unintentional exclusion of high-frequency dynamics, generally take many forms,[17] of which the most commonly used is the multiplicative uncertainty model. Depending on where the errors are reflected with respect to the plant, they are further classified into input and output multiplicative uncertainties. If $\Delta_{im}(s)$ represents a proper and stable approximation transfer function error, then the plant transfer function $[Q(s)]$ from u to y_1 (Fig. 5) perturbed with an input multiplicative uncertainty model is given as

$$Q^*(s) = Q(s)[1 + \Delta_{im}(s)] \tag{11}$$

For simulation and analysis purposes, an approximate model of uncertainty is constructed based on the error from neglecting store aerodynamics. It is derived based on the argument that had the store aerodynamics been included then the circulatory aerodynamics of wing and store combination [as op-

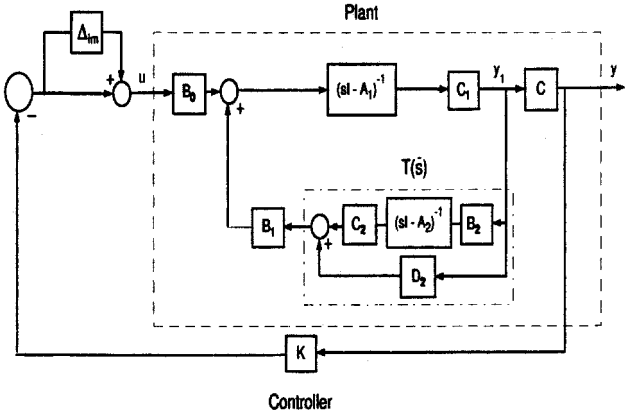

Fig. 5 Block diagram of active flutter suppression.

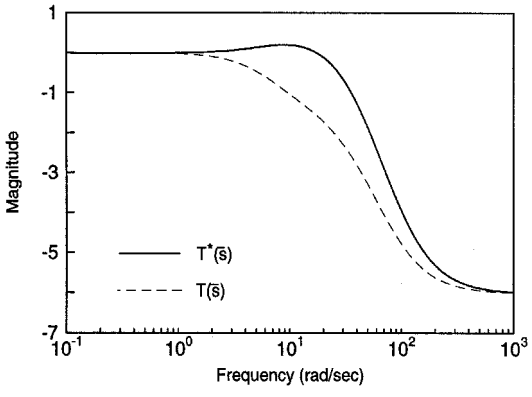

Fig. 6 Jones' approximations.[16]

posed to that of the wing alone as in Eq. (5)] can be approximated by Eq. (5) with the exception that the Jones' rational function be replaced by some Jones'-like transfer function that closely captures the circulatory effects caused by wing/store combination aerodynamics. In other words, the uncertainty in store aerodynamics is reflected on to the uncertainty in Jones' rational function approximation. Here it is assumed that the Jones' approximation $[T(\bar{s})]$ be replaced with a Jones'-like rational approximation $[T^*(\bar{s})]$, whose frequency response characteristics are shown in Fig. 5, where

$$T^*(\bar{s}) = \frac{0.5(sb/U)^2 + 0.3398(sb/U) + 0.013627}{(sb/U)^2 + 0.3455(sb/U) + 0.01365} \tag{12}$$

It is assumed that the majority of the differences between the magnitudes occur in the mid- to high-frequency range. The goal here is to construct an approximate uncertainty model $\Delta_{\text{im}}(s)$ to represent the unmodeled store aerodynamics later used to perturb the closed-loop to evaluate its robustness to modeling limitations. The uncertainty model $\Delta_{\text{im}}(s)$ can now be constructed from the block diagram in Fig. 6 as follows. This block diagram reiterates the fact that flutter is a self-excited phenomenon occurring primarily because of the circulatory aerodynamic loads being regeneratively fed back into the system. Using the Jones' approximation[16] to the Theodorsen's function, the transfer function from u to y_1 can be represented as

$$Q(s) = \frac{\boldsymbol{C}_1[s\boldsymbol{I} - \boldsymbol{A}_1]^{-1}\boldsymbol{B}_0}{1 - \boldsymbol{C}_1[s\boldsymbol{I} - \boldsymbol{A}_1]^{-1}\boldsymbol{B}_1 T(\bar{s})} = \frac{N_0(s)/M(s)}{1 - T(\bar{s})N_1(s)/M(s)} \tag{13}$$

Let the actual plant's transfer function (obtained by using the Jones-like approximation) be given by

$$Q^*(s) = \frac{\boldsymbol{C}_1[s\boldsymbol{I} - \boldsymbol{A}_1]^{-1}\boldsymbol{B}_0}{1 - \boldsymbol{C}_1[s\boldsymbol{I} - \boldsymbol{A}_1]^{-1}\boldsymbol{B}_1 T^*(\bar{s})} = \frac{N_0(s)/M(s)}{1 - T^*(\bar{s})N_1(s)/M(s)} \tag{14}$$

Using the input multiplicative uncertainty, the true plant can be expressed in terms of the nominal plant as

$$\frac{N_0(s)}{M(s) - N_1(s)T^*(\bar{s})} = \frac{N_0(s)}{M(s) - N_1(s)T(\bar{s})}[1 + \Delta_{\text{im}}(s)] \tag{15}$$

The uncertainty model $\Delta_{\text{im}}(s)$ can now be written as

$$\Delta_{\text{im}}(s) = \frac{N_1(s)[T^*(\bar{s}) - T(\bar{s})]}{M(s) - N_1(s)T^*(\bar{s})} \tag{16}$$

which remains the same when an output multiplicative uncertainty model is considered. Because the control theory[17] requires that $\Delta_{\text{im}}(s)$ be stable, the uncertainty model is designed at a flight speed of $0.9U_f$, which is in the subcritical flutter region.

Controller Synthesis

Linear optimal control laws are used to design controllers for the single-input multioutput linear time invariant aeroelastic system of equations that was derived earlier. In this analysis the plant is augmented with a set of integrators at each output channel to ensure zero steady-state tracking errors. The augmented model is represented as

$$\begin{aligned} \boldsymbol{x}_a &= \boldsymbol{A}_a\boldsymbol{x}_a + \boldsymbol{B}_a u + \boldsymbol{\Gamma}_a v \\ \boldsymbol{y}_a &= \boldsymbol{C}_a\boldsymbol{x}_a + \boldsymbol{n} \end{aligned} \tag{17}$$

An LQR technique is initially used where the optimal regulator problem is to find a control input $u(t)$ defined on $[0, \infty]$, which drives the states $\boldsymbol{x}_a(t)$ to zero in an arbitrarily short time. The optimal full-state feedback gain required to achieve this task is obtained by minimizing a scalar performance index $J = \frac{1}{2}\int_0^\infty (\boldsymbol{x}_a^T\boldsymbol{Q}_c\boldsymbol{x}_a + u^T R_c u)\,\mathrm{d}t$, where the positive definite matrix $[\boldsymbol{Q}_c]$ represents the penalty on the states, and $[R_c]$ is a weighting that penalizes the control effort. Minimization is achieved by solving the steady-state algebraic Riccati equation (ARE) for a semipositive definite matrix $\boldsymbol{P}$

$$\boldsymbol{0} = \boldsymbol{A}_a^T\boldsymbol{P} + \boldsymbol{P}\boldsymbol{A}_a - \boldsymbol{P}\boldsymbol{B}_a\boldsymbol{R}_c^{-1}\boldsymbol{B}_a\boldsymbol{P} + \boldsymbol{Q}_c \tag{18}$$

The final optimal gain matrix is then given by $\boldsymbol{K}_c = R_c^{-1}\boldsymbol{B}_a^T\boldsymbol{P}$, and the required control input $u(t)$ is equal to $-\boldsymbol{K}_c\boldsymbol{x}_a(t)$.

Slow variations of store parameters such as mass and the c.g. location are quite common during maneuvers of a high-performance military aircraft. While the LQR design provides a controller robust enough to withstand such low-frequency parameter changes, the unavailability of all states for feedback makes the design impracticable.

As an alternative, a LQG design, which uses noise-corrupted outputs for feedback, is used as a controller. The practicality of the LQG design also lies in the assumption that the uncertainty is represented as an additive white noise. It is assumed that additive process noise v and the measurement noise n [Eq. (17)] are uncorrelated zero-mean, Gaussian, white-noise processes with intensities $\boldsymbol{\Gamma}_a Q_0 \boldsymbol{\Gamma}_a^T$ (positive definite) and R_0 (positive definite). To obtain the estimates $\hat{\boldsymbol{x}}_a$ of the states $\boldsymbol{x}_a(t)$ under noisy measurements, the variance of the error $\tilde{\boldsymbol{x}}_a(t) = \boldsymbol{x}_a(t) - \hat{\boldsymbol{x}}_a(t)$, given by $J_e = E[\tilde{\boldsymbol{x}}_a^T(t)\tilde{\boldsymbol{x}}_a(t)]$, is minimized. Under the standard assumptions that the pair $(\boldsymbol{A}_a, \boldsymbol{B}_a)$ is stabilizable

and (C_a, A_a) is detectable, the state-space representation for the Kalman filter is given by

$$\dot{\hat{x}}_a = A_a\hat{x}_a + B_a u + K_e(y_a - C_a\hat{x}_a) \tag{19}$$

The filter algebraic Riccati equation (FARE) needed to solve for the estimation error covariance Σ is given by

$$0 = A_a^T\Sigma + \Sigma A_a - \Sigma C_a^T R_0^{-1} C_a\Sigma + \Gamma_a Q_0 \Gamma_a^T \tag{20}$$

The Kalman filter gain matrix is then given by $K_e = \Sigma C_a^T R_0^{-1}$. Tuning parameters Q_c, R_c, Q_0, and R_0 can be adjusted until a satisfactory design is obtained. Here the loop is assumed to be broken at the input to reflect all of the uncertainties at the input of the plant, which is also roughly equivalent to the assumption of an imperfect actuator.

Although the LQG design is more practical because it involves the estimation of unknown states and it has the ability to withstand errors caused by unstructured uncertainties, it does not, however, have the desired properties of LQR, namely good nominal performance. To obtain a design that is tolerant of modeling errors and maintains a satisfactory nominal performance, a robust loop-shaping technique, called the loop transfer recovery (LTR), is used.

This LTR technique[18] involves tuning the Kalman filter to recover the stability margins associated with full-state feedback design. The Kalman filter in the LQG technique was designed assuming that it had accurate knowledge of the input. But, in reality, the input has uncertainties (because of unmodeled actuator dynamics) that may not allow the Kalman filter to perfectly estimate the states. Hence, to achieve a perfect estimation of states for input uncertainties, the Kalman filter is redesigned by adding fictitious noise on the input through the B_a matrix, resulting in a modified process noise intensity

$$Q_f = \Gamma_a Q_0 \Gamma_a^T + m_f^2 B_a B_a^T \tag{21}$$

There is, however, no change in the measurement noise weighting that is equal to its original intensity R_0. When $m_f = 0$, the original Kalman filter of Eq. (20) is obtained. Therefore, the loop gain of the modified LQG system becomes $K_c\Phi B_a$, which is equal to that of the LQR. Thus, as m_f is increased, the loop properties of the observer-based system approach that of the LQR design. But if the measurements are much noisier than expected (as indicated by R_0), then the Kalman filter would produce noise-corrupted estimated states and, therefore, would suffer inaccuracy. Thus, there is always a tradeoff between filter accuracy and loop recovery.

Results and Discussion

The values used for simulation purposes are $Q_c = \text{diag}(10^7[1.7, 0.7, 0.03, 0, \ldots, 0])$, $R_c = 2.2 \times 10^{-4}$, $Q_0 = 10^4$, and $R_0 = I_3$. An initial estimate for the state-to-control weighting ratios were based on Ref. 19. The value of m_f is increased from 0, which corresponds to the LQG design to 1×10^3 where the recovery process is stopped. This is based on comparison of the maximal control-input energy constraint (not shown) of the LQG/LTR and $\mathcal{H}_\infty$ controller-compensated systems.[20]

Robust Stability

By applying the small gain theorem[18] to the loop of Fig. 5, a sufficient condition for robust stability, namely, $\bar{\sigma}[\Delta_{\text{im}}(s)]\bar{\sigma}[T(s)] < 1$, can be obtained where $T(s) = K(s)G(s)/[I + K(s)G(s)]$ is the input complementary sensitivity transfer matrix. Assuming the product of $K(j\omega)$ and $G(j\omega)$ to be nonsingular, the stability condition can be rewritten as

$$\bar{\sigma}[\Delta_{\text{im}}(j\omega)] < \underline{\sigma}\{I + [K(j\omega)G(j\omega)]^{-1}\} \tag{22}$$

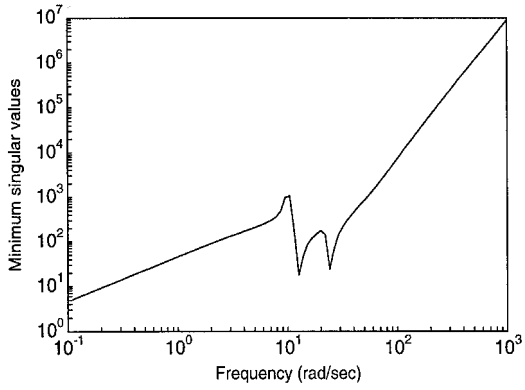

Fig. 7 Tolerance margins vs frequency.

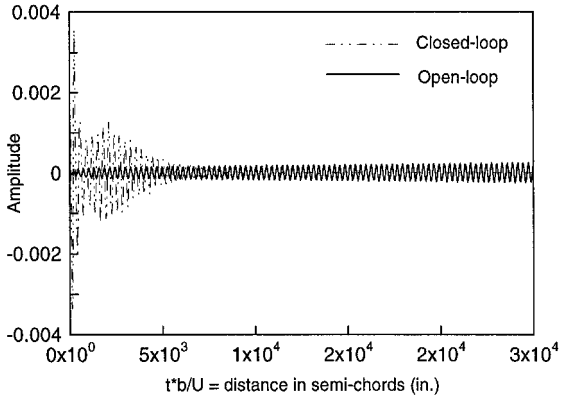

Fig. 8 Step input responses of the original and multiplicatively perturbed systems (output α).

which gives percentage tolerance bounds for input multiplicative uncertainties. The frequency response of the robust stability margins for unstructured uncertainties for each of the outputs is shown in Fig. 7. The absolute value of the minimum singular value of $\{I + [K(j\omega)G(j\omega)]^{-1}\}$ is observed to be 13.44 dB, which implies that the closed-loop system is capable of withstanding at least ±235% plant uncertainty (with errors reflected at the input), without being destabilized. At the flutter frequency (25 rad/s), the magnitude of the stability margin is observed to be ±350%, where the closed-loop system is required to alleviate the effects of modeling limitations, such as those caused by wing/store aerodynamic and other flutter critical uncertainties. For frequencies beyond 25 rad/s, the % tolerance bounds increase monotonically with the increase in frequency. Large endurance margins are necessary at such frequencies where the effects of ignoring aileron degrees of freedom and other flexible modes including sensor and actuator dynamics are prominent.

To test the effectiveness of the controller in sustaining any errors caused by unmodeled dynamics, the input multiplicative model developed earlier [Eq. (16)] is used to perturb the system and the resulting step responses are calculated. A representative time response of the output α is shown in Fig. 8. Clearly, the closed-loop withstands and stabilizes the perturbation, whereas the open-loop system response diverges leading to instability.

Nominal Performance

The singular-value Bode plot of the output sensitivity transfer matrix $S(s) = I/[I + G(s)K(s)]$, which gives a measure of nominal performance, is plotted in Fig. 9. This figure illustrates that the output h of the compensated system is capable of withstanding parameter variations of low- to midfrequency range (<10 rad/s) without amplifying the magnitude of the resulting response. Outputs alpha and theta, however, demonstrated neither

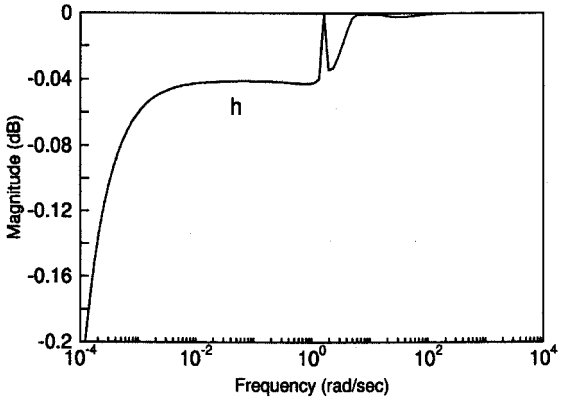

Fig. 9 Singular-value Bode plot of output sensitivity function.

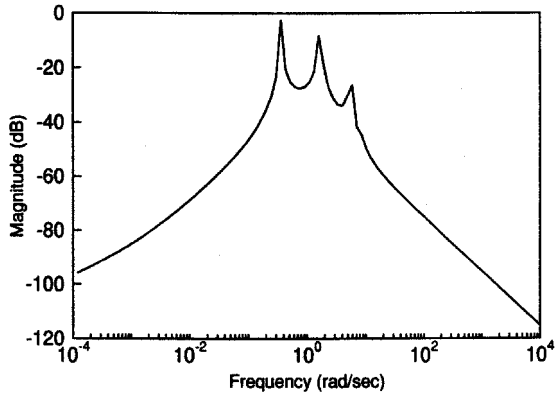

Fig. 10 Frequency response from disturbance input to output (open/closed-loop system).

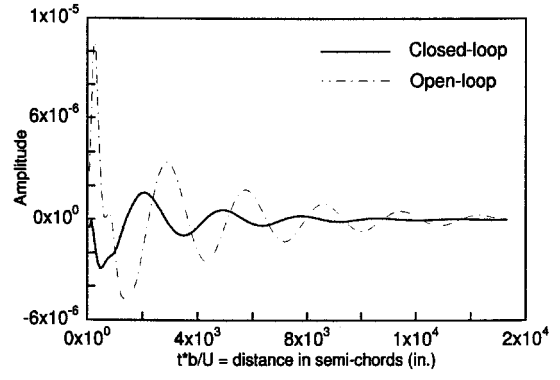

Fig. 11 Output (h) response to step input.

attenuation nor amplification of the sensitivity magnitude (not shown). The frequency response characteristics of the sensitivity function is also equivalent to that of the transfer function (matrix) between the disturbance input (entering at the output of the plant) to the output. In this case, the closed-loop system rejects output disturbances by as much as 0.2 dB at low frequencies.

Another performance measure used to evaluate the effectiveness of the closed-loop system is the frequency response of the transfer function from the disturbance input (entering at the input of the plant) to the outputs. One of the examples is the gust disturbance that typically enters at a low frequency of around 6 rad/s. To compare the performance of the open- and the closed-loop systems to a sinusoidal disturbance input, the controller is designed at $0.9U_f$, using the same control parameters used earlier. A plot of the frequency response of the transfer matrix from the disturbance input to the output is shown in Fig. 10. Clearly at all frequencies, the frequency response of the two systems exactly overlap, indicating that no attenuation can be expected in the maximum magnitude of the disturbance. In the time domain (not shown), except for faster transient response and smaller settling time, no reduction was obtained in the peak amplitude—an issue that needs to be addressed. Finally, Fig. 11 compares the output h response of the closed-loop system to that of the open-loop system for step inputs with controller designed at $0.9U_f$. It clearly shows that the output has better responses in terms of transient amplitude reduction and settling time.

Conclusions

A loop transfer recovery algorithm has been applied to demonstrate the feasibility of designing a controller to enhance the performance and improve the stability robustness of an active wing/store flutter suppression system. A piezoceramic wafer actuator strut is proposed for use as an active decoupler pylon between the wing and the store. The closed-loop simulations showed potential benefit in terms of improving robustness to high-frequency unstructured uncertainties such as those because of limitations posed by modeling store aerodynamics and other flexible modes. Overall, an increase in the nominal performance in terms for transient response and settling time for step inputs have been observed with the control system. In addition, relative to the open-loop system, the output h of the closed-loop demonstrated insensitiveness to low-frequency parameter variations. Potential concerns are the lack of sensitivity attenuation magnitudes at the pitch angle outputs and the inability of the compensated system to reject any external disturbances. In addition to investigating the actuator limitations such as stroke length and power requirements, future study would include extending the concept into the subsonic range and addressing the store-release problem.

Acknowledgment

The authors are grateful for the generous support of the U.S. Air Force Office of Scientific Research, F49620-95-1-0362, under the direction of Brian Sanders.

References

[1]Mykytow, W. J., "Recent Analysis Methods for Wing/Store Flutter," *Specialist Meeting on Wing-with-Stores Flutter*, CP-162, AGARD, April 1962.

[2]Triplett, W. E., "A Feasibility Study of Active Wing/Store Flutter Control," *Journal of Aircraft*, Vol. 9, No. 6, 1972, pp. 438–444.

[3]Noll, T. E., Felt, L. R., Mykytow, W. J., and Russell, H. L., "Potential Application of Active Flutter Suppression to Future Fighter Attack Aircraft," *Aircraft/Stores Compatibility Symposium Proceedings*, Vol. V, 1973, pp. 18–20.

[4]Sandford, M. C., Abel, I., and Gray, D. L., "Development and Demonstration of a Flutter Suppression System Using Active Controls," NASA TR-R-450, Dec. 1975.

[5]Harvey, C. T., Johnson, T. L., and Stein, G., "Adaptive Control of Wing/Store Flutter," Air Force Flight Dynamics Lab., TR-79-3081, April 1979.

[6]Haidl, G., Lotze, A., and Sensburg, O., "Active Flutter Suppression on Wings with External Stores," AGARD, AG-175, 1974, pp. 57–74.

[7]Hönlinger, H., "Active Flutter Suppression on an Airplane with Wing Mounted External Stores," AGARD, CP-228, Aug. 1977.

[8]Hönlinger, H., and Destuynder, R., "External Store Flutter Suppression with Active Controls," *Lecture Series*, Vol. 2, von Kàrmàn Inst. for Fluid Dynamics, Dec. 1978, pp. 1–85.

[9]Reed, W. H., III, Foughner, J. T., Jr., and Runyan, H. L., "Decoupler Pylon: A Simple Effective Wing/Store Flutter Suppressor," *Journal of Aircraft*, Vol. 17, No. 3, 1980, pp. 206–211.

[10]Triplett, W. E., Kappus, H. P. F., and Landy, R. J., "Active Flutter Suppression Systems for Military Aircraft—A Feasibility Study," U.S. Air Force Flight Dynamics Lab., TR-72-116, Feb. 1973.

[11]Clayton, J. D., Haller, R. L., and Hassler, J. M., Jr., "Design and Fabrication of the NASA Decoupler Pylon for the F-16 Aircraft," NASA CR-172354, Jan. 1985.

[12]Gade, P. V. N., and Flowers, G. T., "Flutter Suppression of an Airfoil with Unsteady Forces Using a Piezoelectric Active Strut," AIAA Paper 94-1746, April 1994.

[13]Pokines, B., Belvin, W. K., and Inman, D. J., "Static and Dynamic Characteristics of a Piezoceramic Strut," *Proceedings of the 5th*

AIAA/DOD Control-Structures Interaction Technology Conference, AIAA, Washington, DC, 1992, pp. 133–140.

[14]Theodorsen, T., "General Theory of Aerodynamic Instability and the Mechanism of Flutter," *Aerodynamic Flutter*, edited by I. E. Garrick, Vol. V, AIAA Selected Reprint Series, AIAA, New York, 1969, pp. 22–31.

[15]Edwards, J. W., "Unsteady Aerodynamic Modeling and Active Aeroelastic Control," Stanford Univ., SUDAAR 504, Stanford, CA, Feb. 1977.

[16]Jones, R. T., "Operational Treatment of the Nonuniform Lift Theory to Airplane Dynamics," NACA TN 667, March 1938, pp. 347–350.

[17]Zhou, K., Doyle, J. C., and Glover, K., *Robust and Optimal Control*, Prentice–Hall, Englewood Cliffs, NJ, 1996, pp. 213–228.

[18]Ridgely, D. B., and Banda, S. S., "Introduction to Robust Multivariable Control," Air Force Wright Aeronautical Labs., TR-85-3102, Feb. 1986.

[19]Venkayya, V. B., and Tischler, V. A., "Frequency Control and Its Effect on the Dynamic Response of Flexible Structures," *AIAA Journal*, Vol. 23, No. 11, 1985, pp. 1768–1774.

[20]Gade, P. V. N., and Inman, D. J., "Two-Dimensional Active Wing/Store Flutter Suppression Using $\mathcal{H}_\infty$ Theory," *Journal of Guidance, Control, and Dynamics*, Vol. 20, No. 5, 1997, pp. 949–955.